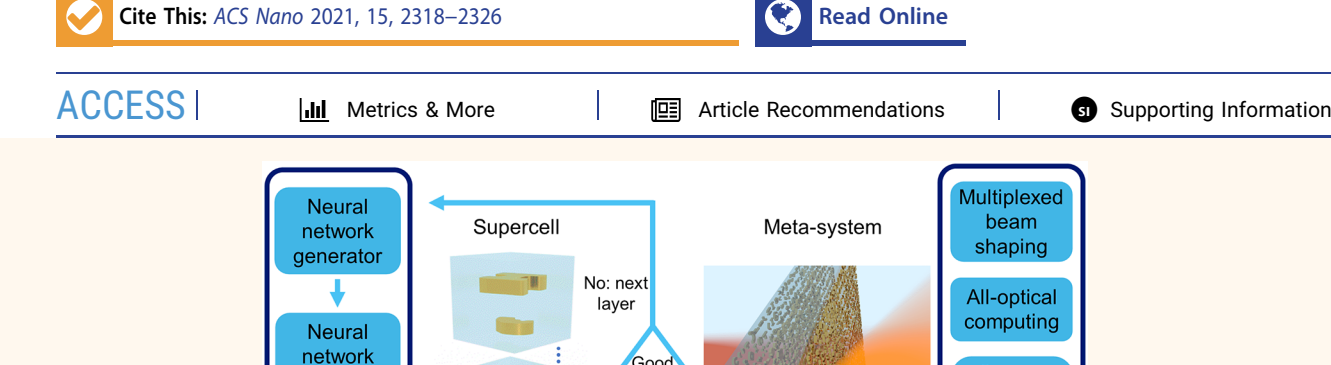


www.acsnano.org

Building Multifunctional Metasystems via **Algorithmic Construction**

Dayu Zhu, Zhaocheng Liu, Lakshmi Raju, Andrew S. Kim, and Wenshan Cai*



Good

results?

Yes: next

supercell

ABSTRACT: Flat optics foresees a promising route to ultracompact optical devices, where metasurfaces serve as the foundation. Conventional designs of metasurfaces start with a certain structure as the prototype, followed by extensive parametric sweeps to accommodate the requirements of phase and amplitude of the emerging light. Regardless of how computation consuming the process is, a predefined structure can hardly realize the independent control over polarization, frequency, and spatial channels, which hinders the potential of metasurfaces to be multifunctional. Besides, achieving complicated and multiple functions calls for designing metasystems with multiple cascading layers of metasurfaces, which introduces exponential complexity. In this work, we present a hybrid deep learning framework for designing multilayer metasystems with multifunctional capabilities. We demonstrate examples of a polarization-multiplexed dual-functional beam generator, a second-order differentiator for all-optical computing, and a space-polarization-wavelength multiplexed hologram. These examples are barely achievable by single-layer metasurfaces and unattainable by traditional design processes.

KEYWORDS: deep learning, metasurface, photonics, neural network, optics

simulator

Evolutionary

optimizer

etasurface is one of the most appealing ideas in nanophotonics in the past decade. 1,2 As the twodimensional counterpart of metamaterials, metasurfaces introduce abrupt phase change to the interface, which empowers the ultrathin layer to function as a bulky optical component. This intriguing advantage allows for numerous applications of metasurfaces, such as metalenses, wavefront shaping, compact imaging, to name a few. 3-6 At the early stage, most optical metasurfaces were implemented through plasmonics, which can achieve the complete phase control of the cross-polarized output wave. Nevertheless, the theoretical limit of the cross-polarized conversion efficiency of plasmonic metasurfaces is only 25%, and the ohmic loss associated with plasmonic metasurfaces further leads to lower efficiency. The other family of metasurfaces, the dielectric ones, can achieve a much higher efficiency and are more compatible with the modern semiconductor industry.8 The transmittance

of nonresonant dielectric metasurfaces can reach near unity in the optical regime, providing high efficiency but mediocre amplitude control. Apart from the individual merit and demerit of plasmonic and dielectric metasurfaces, most metasurfaces are built upon single-layer unit cells, which have rather low degrees of freedom (DOF) to accomplish a sophisticated objective. For instance, a single-layer metasurface can hardly be highly multifunctional, since the optical responses of a unit cell at different polarizations, frequencies, and spatial positions are correlated with each other, which cannot be treated as

Space-

oolarization. wavelength

multiplexed

holography

Received: November 10, 2020 Accepted: January 6, 2021 Published: January 8, 2021





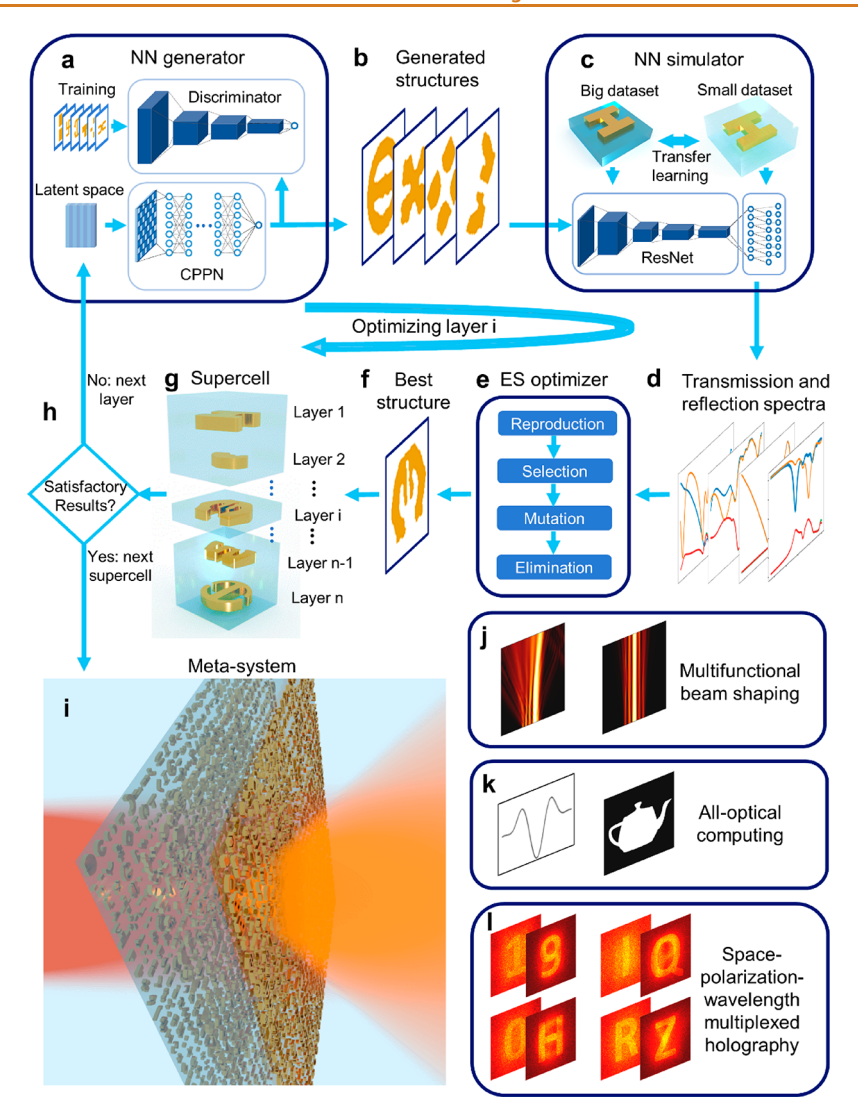


Figure 1. Description of the modules of the DL framework. The design flow goes through the NN generator, the NN simulator, and the ES optimizer in a loop. The generator is a CPPN of a GAN. The simulator is trained sequentially through transfer learning. The workflow proceeds as follows: the generator (a) first decodes a batch of latent vectors and produces corresponding candidate nanostructures (b), followed by the NN simulator (c) computing the transmittance and reflectance spectra of the nanostructures (d). Next, the ES optimizer (e) selects the structures with satisfactory performance, refines and evolves their latent vectors, and sends the latent vectors back to the generator to get a better batch of nanostructures (f–h). Different layers at the same position can be collectively viewed as a supercell (g). One layer of the supercell is optimized in every single iteration, and the design proceeds in a round-robin fashion until the overall performance of the supercell is satisfactory (h). The design of the metasystem (i) terminates when all the spatially variant supercells are obtained. The metasystem can be designed as a multifunctional optical device, for applications such as multifunctional beam shaping (j), operators for all-optical computing (k), and space-wavelength-polarization multiplexed holography (l).

independent channels to multiplex information. Trials are made to design multifunctional metasurfaces by integrating several types of nanostructures onto one metasurface, ^{9–11} where each type of nanostructure functions toward a distinct objection. However, this scheme may impede the resolution of metasurfaces, and the crosstalk between nanostructures is unavoidable. These limitations of metasurfaces call for a metasystem with multiple metasurfaces to fulfill a complicated objective, analogous to an optical system with cascading lenses. In this sense, a metasystem is a favorable choice for implementing highly multifunctional devices.

The metasystem can be intuitively viewed as multiple layers of metasurfaces, with a subwavelength total thickness. ^{12,13} Nevertheless, most multilayer metasurfaces regard each layer as an individual device, and the ultimate performance can be calculated through ray-tracing or other methods. In contrast to

the general idea of multilayer metasurfaces, here we introduce the multilayer metasystem, which does not necessarily require each layer to have a distinct function. Hence, we only need to design the entire system toward the ultimate objective without distinguishing the layer-wise properties. Besides, the metasystem also bridges the gap between plasmonic and dielectric metasurfaces. For one thing, the metasystem provides sufficient propagation length for waves, similar to dielectric metasurfaces, which aids the full coverage of phase. For another, the metasystem can be composed of either metals or dielectrics, or both, to achieve complete amplitude modulation. In addition, high DOF of the metasystem provides independent control of the optical responses of different multiplexed channels. The microscopic patterns of such metasystems can be as complicated as arbitrary geometries, which further improves the DOFs. 14 In this article, we will demonstrate that

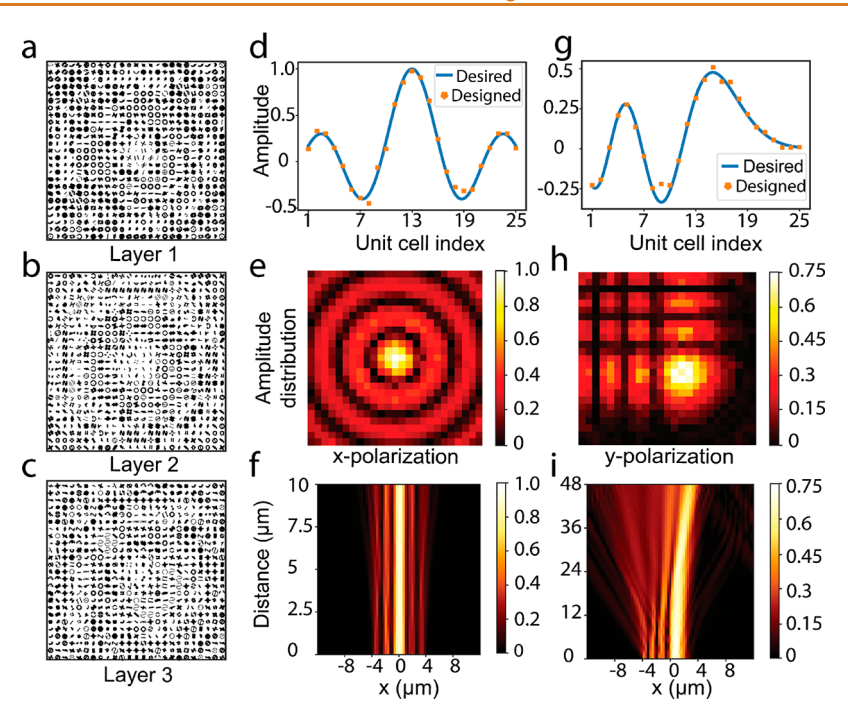


Figure 2. DL designed metasystem as a polarization-multiplexed dual-functional beam generator. When the incident light is x-polarized, the transmitted x-polarized wave forms a Bessel beam, while y-in-y-out response is an Airy beam. (a-c) Detailed structure of the metasystem. The system has three layers (a-c), each layer consists of 25×25 unit cells. The light incidence is on the layer 1 side and output on the layer 3 side. (d and g) Desired amplitude distributions (blue) and simulated amplitudes (orange) of the metasystem on the central axis, for the x-polarized and the y-polarized incidence, respectively. (e and h) Simulated amplitude distributions of the light field on the output plane, for the x- and y-polarized incidence, respectively. (f and i) Simulated amplitude distributions of the transmitted light along the propagation z direction, for the x- and y-polarized incidence, respectively.

metasystems can be one of the best candidates to achieve multifunctional purposes for light waves. As for analog computing applications such as all-optical computing, signal and imaging processing, pattern recognition, *etc.*, metasystems also represent one of the most promising media.

Meanwhile, increased design complexity is coexistent with the advantages of the metasystem. The conventional design process requires a predefined nanostructure as the building block, then a thorough sweep of the geometric parameters of the nanostructure is necessary. This design flow suffers two major shortcomings when applied to metasystems. One is that the selected nanostructure may not cover the solution space of the desired functions. For instance, predefining a nanostructure with distinct functionality at different wavelengths is never a closed form question, and tedious trial-and-error attempts to vary the parameters of the nanostructure is usually necessary, but with no guarantee of a solution. The other is that adding layers will increase the number of parameters exponentially. Therefore, the parameter-scanning process will consume huge computational resources and storage, which is unacceptable or even impractical. This dilemma can be perfectly mitigated by our hybrid deep learning (DL) framework. Advances in neural networks (NNs) and computational hardware have given birth to diverse applications of DL in information technology, 15-17 such as pattern recognition, natural language processing, autonomous vehicles, etc. Besides, DL also benefits the methodology of natural science, ^{18–20} including biology, chemistry, quantum mechanics, as well as optics and nanophononics. Recently, the interdisciplinary regime between optics and DL has caught intense attention. Various studies have validated the potential of leveraging DL for the design of optical components and proven that DL design methods can

essentially outperform traditional human design processes on certain tasks. ²¹⁻³³ It is worth noting that researchers to date may have not paid enough attention to the tasks with formidably high complexity, which are hardly resolvable by conventional design processes and thus exclusive to DL design methods. In this work, we introduce the DL framework for the discovery and design of a multilayer multifunctional metasystem, which is too complicated to be accomplished through conventional design processes. As solid illustrations, we report three examples designed by our framework: a polarizationmultiplexed dual-functional beam generator, a second-order differentiator for all-optical computing, and a space-polarization-wavelength multiplexed hologram. These functions are barely achievable by single-layer metasurfaces, and the devices are hardly approachable by conventional design means. The designed devices are constituted of arbitrary patterns, which indicates the extremely high DOFs of the structures involved.

RESULTS AND DISCUSSION

Pipeline of the DL Framework. The design flowchart of our DL framework is presented in Figure 1. The algorithm architecture consists of a NN generator,³⁴ a NN simulator,³⁵ and an evolutionary strategy (ES)-based optimizer.³⁶ As the design initiates, the compositional-pattern generating network (CPPN) generator decodes a batch of latent vectors and produces corresponding candidate nanostructures,³⁷ followed by the ResNet-based simulator computing the optical responses of those nanostructures.¹⁷ It is worth noting that the simulator is trained with a tiny data set through transfer learning to reduce the data requirement and maintain a high accuracy. Here, we assume all the nanostructures have a unit size of 320 nm and thickness of 40 nm, embedded in polymer

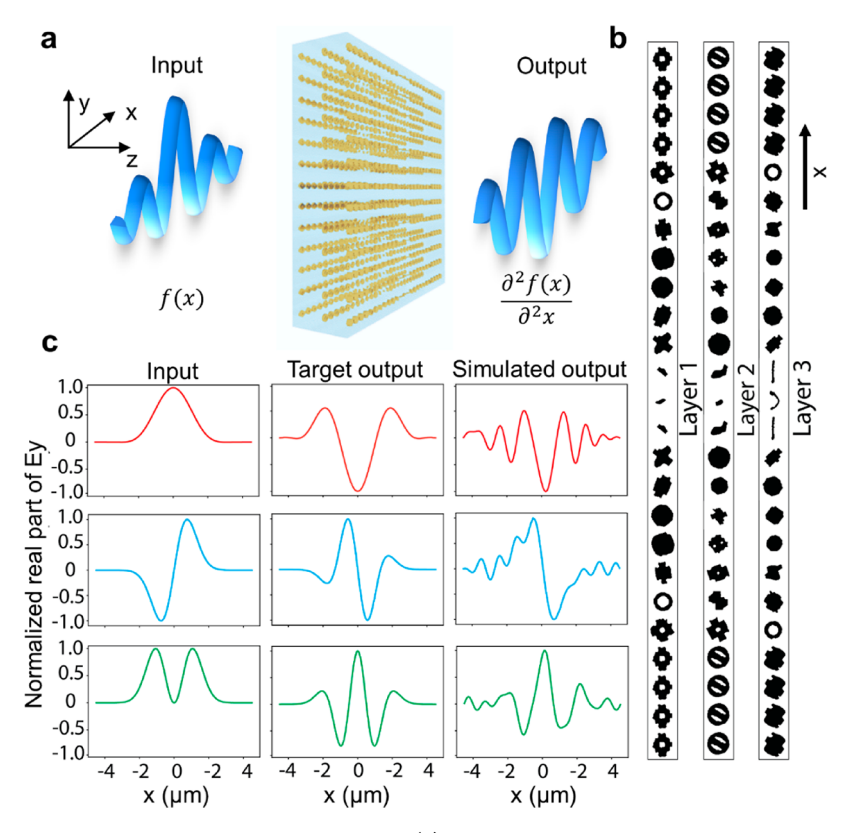


Figure 3. DL designed metasystem for second-order differentiation. (a) Schematic of the function of the second-order differentiator. When the input is a wave with a spatially variant real part along the *x* direction, the real part of the output wave will be the second-order derivative of the input. (b) Detailed structure of the metasystem. Each layer of the trilayered system has 25 spatially variant unit cells along the *x* direction and is periodic along the *y* direction. The incidence is on layer 1 side, and the output is on layer 3 side. (c) Three examples to test the functionality of the differentiator. The left column is three examples of the input, while the middle and right columns are the target output and the actual output of the meta-optic second-order differentiator, respectively. Since the differentiator has only 25 unit cells along the *x* direction, the resolution of the differentiation is limited, which leads to the ripples in the simulated output.

with refractive index of 1.57. Next, the ES optimizer selects the structures with good performance, refines and evolves their latent vectors, and sends the latent vectors back to the generator to get a better batch of structures. The optimizer regards unit cells at the same planar position but on different layers as one supercell collectively, and the procedure proceeds as a loop until a satisfactory supercell is obtained (e.g., mean-square-error between the objective and the achieved performance is lower than 0.01), then the framework will work on designing the supercells at other planar positions. Generally, designing a three-layered supercell takes no more than 5 min, which is much more efficient than parametric sweeping methods. Detailed descriptions of the framework are presented in the Methods section.

Dual-Functional Polarization-Multiplexed Beam Generator. The first case study of the DL designed metasystem is a dual-functional beam generator, as shown in Figure 2. When the incident light is an *x*-polarized plane wave, the transmitted *x*-polarized output represents the zeroth-order Bessel beam, while the *y*-in-*y*-out response is an Airy beam. Beam shaping is a classical application of metasurfaces, by which the ultrathin beam generator is feasible, while bulky optical components, such as axicons and lenses, are no longer necessary. Beam shaping calls for a spatially variant magnitude and phase of the output light, and polarization-dependent functions further increase the design complexity. This task is too complicated for traditional design processes or single-layered metasurfaces, so one promising solution is to implement the DL algorithm to

design a multilayer metasystem with target multifunctional properties. Without loss of generality, we preset the metasystem to possess three layers, with 25 spatially variant supercells in both α and γ directions, and the polymer spacer between adjacent layers is set to 200 nm. The wavelength here is 659 nm in the polymer, which is randomly chosen to validate the performance of our algorithm. Upon settling down the amplitude and phase requirements and the physical parameters, the framework will generate the best possible supercells at each planar position. The full-wave simulation is further used to validate the design efficacy.

The details of the dual-functional Bessel-Airy beam generator are displayed in Figure 2. Figure 2a-c depicts the detailed structure of each layer, from the top layer to the bottom, respectively, and we assume the incidence light illuminates from the top. Some of the complicated patterns can be smoothed by applying denoising and Fourier filter algorithms to extract the main features without compromising the device performance, as the tiny details of the structures do not contribute much to the far-field distributions. The detailed discussion concerning the shape tolerance in experiment is provided in the Supporting Information, and this work mainly focuses on the DL algorithm and uncovers the promising merits of metasystems. Figure 2d,g demonstrates the comparison between the amplitude distributions of designed and target transmittances for the two polarizations on the central axis of the beam generator, which reveals the notable agreement between the achieved and target performance. For

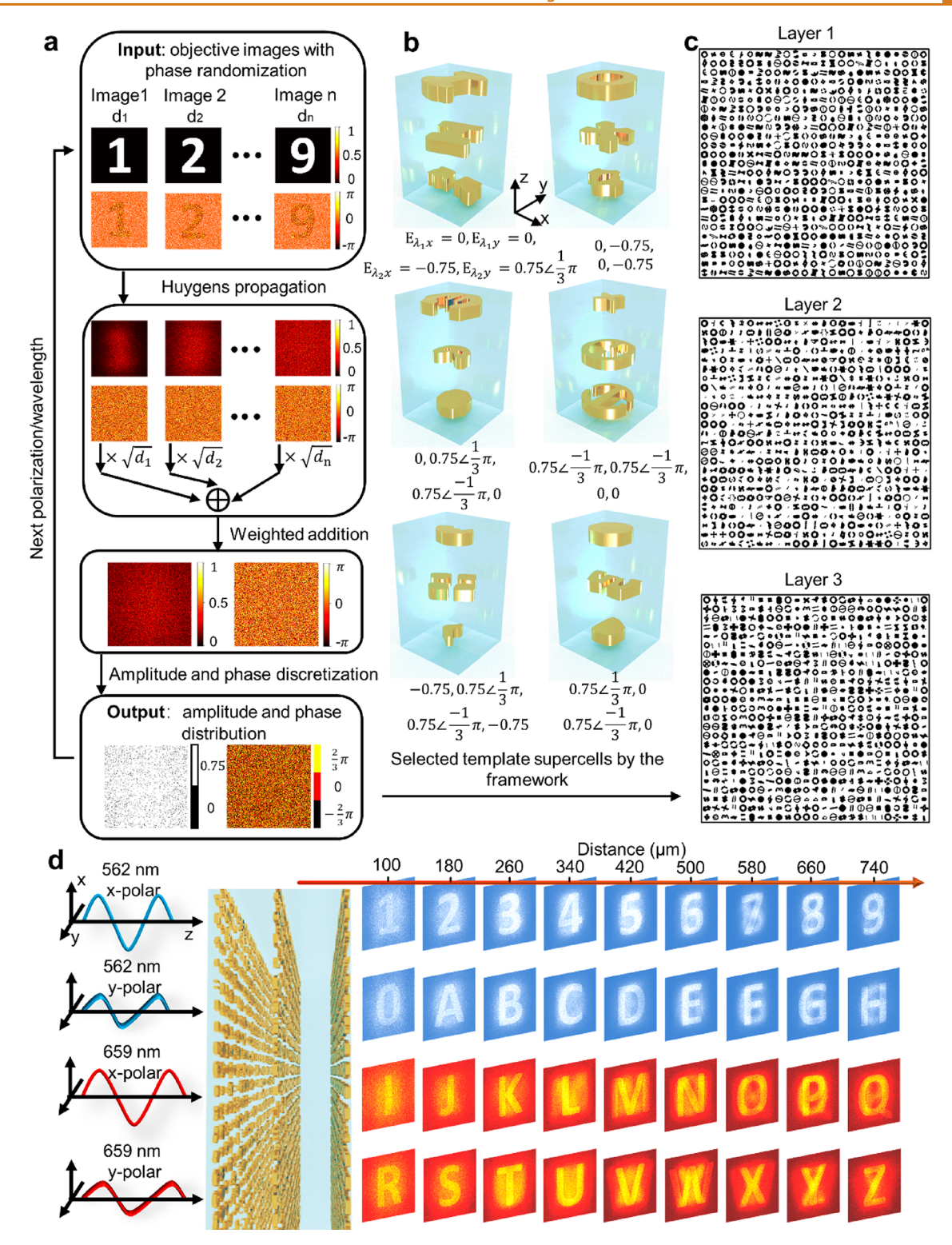


Figure 4. DL designed space-polarization-wavelength multiplexed hologram. The hologram can project 36 different holographic images in total. (a) The flowchart to obtain the amplitude-and-phase distributions of the design objective. The first step is to pin down the target images projected by the hologram and their distances to the hologram plane, then random phases are added to each of them. Next, their projected amplitude and phase distributions on the hologram plane are computed by the Huygens propagation, the weighted superposition is calculated, and then the amplitude is normalized to between 0 and 1. Lastly, the amplitude and the phase are discretized. The hologram functions at two wavelengths and two polarizations, which means the process should be carried out four times to get all the distributions. (b) Some examples of the designed supercells. Their target responses at x and y-polarized incidence at 562 nm (λ_1) and 659 nm (λ_2) in the polymer are denoted as $E_{\lambda_1x}E_{\lambda_2y}E_{\lambda_2x}E_{\lambda_2y}$. (c) A part of the designed hologram. The total hologram consists of 2000 \times 2000 trilayered supercells, and here we display a locality of 25 \times 25 supercells. The incidence is on layer 1 side and output on layer 3 side. (d) Simulated performances of the hologram. The hologram works at both x and y polarizations, 659 and 562 nm, and the projected images are at 9 distances to the hologram, from 100 to 740 μ m. The projected 36 images are the numerical digits 0–9 and capital letters A–Z.

the whole metasystem, the average design accuracy of the optical responses of the supercells can reach approximately 90%, which guarantees the effectiveness of the designed dualfunctional beam generator. Figure 2e,h presents the simulated output of the beam generator at x and y polarizations, respectively, where the light field distributions undoubtedly represent the desired Bessel and Airy patterns. The simulated light propagations are illustrated in Figure 2f,i, where the nondiffracting characteristics of both beams and the selfbending of the Airy beam are evidenced. Besides being multifunctional, the designed beam generator exhibits a decent efficiency compared to beam generators by conventional plasmonic metasurfaces. For x-polarized incidence, assuming an input intensity of 100%, the peak intensity of the transmitted Bessel beam reaches 98%. For y-polarized incidence, since the peak value of an Airy function is not unity, to reveal the capability of our DL algorithm, we randomly choose 50% as the peak value of the objective Airy beam on the central axis, as indicated in Figure 2d. Our design fulfills the objective as expected, and the peak intensity of the transmitted Airy beam is approximately 55%. Compared to conventional plasmonic metasurfaces with a theoretical upper limit of 25% transmitted power, the designed metasystem achieves far superior efficiency.

All-Optical Second-Order Differentiator. The second example of the DL designed multilayer metasystem is a second-order differentiator, which is a representative example of all-optical computing and all-optical signal processing. Calculation and signal processing with metasurfaces has long been an intriguing topic to achieve all-optical computing 13,38-42 A number of approaches have been proposed on this subject, however, some require design of a metasurface and two bulky gradient-index structures independently, and others are based on multilayer homogeneous metamaterials but only applicable to math operations with even symmetry and the design may need too many layers or unrealistic materials. Inspired by the theoretical background of the multilayer metamaterial method, we can exploit the metasystem to realize certain functions for all-optical computing. The metasystem is an ideal candidate to achieve the spatially variant Green's function, which represents wavenumberdependent transmittance in k-space. Since the spatially distributed supercells are not necessarily symmetric, the metasystem can be adapted to any linear operation, such as derivation, integration, convolution, etc.

In our example of metasystem for second-order differentiation, the schematic of the three-layered computing metasystem is illustrated in Figure 3a. In this showcase, when the incident light (659 nm in the polymer) is y-polarized with the real part of the electric field as a spatially distributed function along the *x*-axis, the real part of the *y*-polarized output wave will be proportional to the second-order derivative of the input function. Figure 3b depicts the structure of the designed metasystem. The system has three layers, each of which has 25 spatially variant unit cells along the x direction and is periodic along the y direction, with a spacer of 200 nm between adjacent layers. We define layer 1 on the input side and layer 3 for output. To evaluate the performance of the differentiator, we tested it with three different inputs. The three images in the left column of Figure 3c present the input functions, while the middle and the right columns represent the corresponding target outputs and the simulated outputs of the metasurface, respectively. The great similarities between the targets and the

simulated results of the device validate the performance of the differentiator. Some minor discrepancies such as the asymmetric features and small ripples in the output may appear in our simulation results. These imperfections stem from the incapability of full wave simulation for handling largesized three-dimensional models as well as the low spatial resolution of the discretized differentiator. Since the metasystem consists of only 25 unit cells along the x direction for the representation and operation of a continuous function, the computational resolution of the differentiation is limited due to the discretization in the spatial domain. Increasing the number of unit cells of the metasurface is expected to substantially suppress the ripples in the simulated output. To take one step forward, if a two-dimensional image is the input, the differentiator will detect the second-order edges of the image along the x direction. While if the differentiator is designed to be spatially variant in two dimensions, it will be able to distinguish all the second-order edges of an input image. As a result, the devices designed by the DL framework are potentially applicable to all-optical image processing, computing, NNs, and more.

Space-Polarization-Wavelength Multiplexed Metahologram. In the last example of multilayer multifunctional metasystems, we present a space-polarization-wavelength multiplexed metasurface hologram. This metahologram functions at the wavelengths (in the polymer) of both 562 and 659 nm, in both x and y polarizations, with 9 operational positions along the propagation, and projects a total of 36 holographic images: numerical digits 0-9 and capital letters A-Z. Metasurface has been exploited as one of the most promising media to achieve holography, with high imaging quality and ultrathin thickness. 43,44 Most of such optical metaholograms are static and monofunctional, which leads to a limited information-storing capacity of the holography. Multiplexed metasurfaces may offer the opportunity to encode an enormous amount of information into a single hologram. Some of the recent works have shown the possibility to realize a multiplexed hologram in the spatial, polarization, or wavelength channel, and some have attempted two of the above channels. 9,10,45,46 Here, we present a multiplexed hologram that utilizes all three channels, with no upper limit on the total amount of displayed images.

The hologram is neither phase only nor amplitude only, but with mixed phase and amplitude information carried in one integrated system. It consists of three layers, with an overall size of 2000 × 2000 supercells. The design flowchart is presented in Figure 4a. We first virtually align all the objective images on axis and parallel to the hologram plane at different distances (100–740 μ m from the metahologram, with 80 μ m interval). While the projected function only pertains to the magnitude of light at the generated images, we still need to introduce a random phase to the images in order to suppress the crosstalk between different image planes. Next, we apply a Sommerfeld-Fresnel transformation (Huygens propagation) to obtain the amplitude and phase distribution on the hologram plane as derived from the image planes.⁴⁷ The final amplitude and phase distribution is the weighted sum of the projections, where the weight is proportional to the square root of the distance from the metahologram to a particular image. The weight is introduced to ensure that each image can be recovered by the hologram with both high fidelity and sufficient brightness. To reduce the computational complexity, the objective field amplitude after the hologram is binarized

into the values of 0.75 or 0 with a threshold of 0.3. The phase is also discretized into three values within the 2π period: $-\pi$, $-\frac{1}{3}\pi$, and $\frac{1}{3}\pi$. Therefore, for each polarization at a specific wavelength, there will be four possible amplitude and phase combinations: 0, -0.75, $0.75 \angle -\frac{1}{3}\pi$, and $0.75 \angle \frac{1}{3}\pi$. Since the hologram is designed to work at two different wavelengths (562 and 659 nm) and two polarization states (x and y polarizations), there are a total of $(4^2)^2 = 256$ amplitude and phase combinations, which means the same number of unique supercells should be used to constitute the metahologram. The detailed structures of the supercells are presented in the Supporting Information, and Figure 4b shows a few representative ones. The numbers below each supercell indicate its target responses under x- and y-polarized incidence at 562 nm (λ_1) and 659 nm (λ_2), denoted as $E_{\lambda_1 x} E_{\lambda_1 y} E_{\lambda_2 x} E_{\lambda_2 y}$. Once the 256 supercells are designed by the algorithm, any hologram that operates for both x and y polarizations at the two wavelengths can be designed in a matter of seconds, since different holograms are simply different maps of the same collection of supercells. In this example, the hologram consists of 2000 × 2000 supercells, and Figure 4c displays a small portion of the overall structure. We assume the incidence light illuminates from layer 1, and the output light beyond layer 3 automatically forms the projected images at the expected locations. Figure 4d shows the 36 simulated holographic images, and the color tones of the images are applied to distinguish the shorter (562 nm, blue) and longer (659 nm, red) operating wavelengths. Most of the holographic images are formed with clear outlines and fine features. The image quality does not degrade at large distances, and the fidelity of images is satisfactory at each polarization and each wavelength. As for the scalability, the 256 unique supercells can be readily adapted to design any space-polarization-wavelength multiplexed holograms for the polarization states and operating wavelengths specified before. Additional examples and further discussions on the performance and capacity of the metahologram are presented in the Supporting Information. It is worth noting that our method can be extended to the design of holograms at more operating wavelengths and image positions. Adding one wavelength with both polarizations will increase the number of unique supercells by 16 times.

CONCLUSIONS

In summary, we have proposed a hybrid DL framework for designing highly complicated, multifunctional metasystems. The framework is of high efficiency and accuracy and requires only a small amount of data and a low computational expense, and the algorithm proceeds automatically with no need for human intervention. It is very versatile and can be applied to other configurations through transfer learning. We have presented three examples designed by the DL framework: a polarization-multiplexed dual-functional beam generator, a second-order differentiator for all-optical computing, and a space-polarization-wavelength multiplexed hologram. These devices are virtually insoluble through a conventional design method, with functions hardly achievable by a single-layer metasurface. We acknowledge that most of the metastructures presented in these examples are highly complicated. Experimental realization of these designs would require demanding aligned lithography techniques to fabricate the delicate arrangements of trilayered supercells. These real-life challenges

can be mitigated to a certain extent if we explore the microwave counterparts of the proposed systems, where the feature size would lie within the millimeter scale. We further note that the primary theme of this research is to reveal the capacity of the machine-learning frameworks for the design and implementation of multifunctional metasystems, while the experimental demonstration of these proposed concepts is beyond the scope of the current work.

The DL framework developed here is also applicable to the design of other photonic components and systems, including photonic crystals, chip-scale silicon devices, and quantum-optical devices. The methodology of our DL design algorithm is also significant to other disciplines of natural sciences, such as the design of nanomaterials, searching for new topological insulators, planning of chemical syntheses, prediction of protein structures, and many more. Consolidating the power of artificial intelligence into scientific research foresees the emergence of novel devices beyond human design capacities, discovers underlying physics from nebulous or counterintuitive observations, and pushes forward the limits of knowledge as we know today.

METHODS

The NN generator is the generative model of a generative adversarial network (GAN). Most GANs are constructed by CNN, which is beneficial to extract the inherent features of images. However, different nanostructures of metasurfaces seldom share common features, so we turn to a CPPN to implement the generator of the GAN, which is proven to be effective for generating artistic patterns with various styles. As for the NN simulator, it is adapted from ResNet18, with 64×64 pixelated images as the input and the complex transmission and reflection spectra (170-600 THz in frequency, corresponding to the wavelength from 500 to 1765 nm in free space) as the output. Each image represents the two-dimensional nanostructure of a unit cell, with a unit cell size of 320 nm and pattern thickness of 40 nm. To be reasonable for multilayer designs, we assume all nanostructures are gold and embedded in a polymer with a refractive index of 1.57. Although the simulator is a very deep NN, it is trained with a tiny data set of only 2000 image-spectra pairs. We avoid simulating the spectra of a gigantic number of nanostructures to generate the training data set by applying transfer learning to reduce the data requirement. Previously we have simulated 16,000 imagespectra data pairs of unit cells of the same size and pattern thickness, where the gold structure is deposited on glass and exposed in air. Although the material configurations are different, transfer learning is capable of identifying the connection. We first use the previous data (air-glass-gold configuration) to train our simulator and obtain 98% accuracy. The accuracy is defined as $1-\frac{1}{\eta_\lambda\eta_p}\sum_\lambda\sum_p\big|\big|E_{\lambda,p}-T_{\lambda,p}\big|\big|,$

where $E_{\lambda,p}$ is the objective complex transmission at wavelength λ and polarization p, $T_{\lambda,p}$ represents the corresponding transmission, and n_{λ} and n_v denotes the numbers of wavelength points and polarization states, respectively. When we consider both x and y polarizations, $n_n =$ 2. After that, with freezing all the network layers of the simulator except for the last layer, we continue training the simulator with only 2000 new data (polymer-gold configuration) and achieve 96% accuracy. The high efficacy of the simulator suggests that transferring learning successfully transfers the knowledge from the air-glass environment to the polymer-embedded environment. It also indicates that our framework can be readily transferred into any other setups of materials or sizes. For instance, while in this work we present examples of plasmonic metasystems, the design framework can be seamlessly adapted for dielectric metasystems. The only revision needed here is to replace the simulator with a new one for dielectric structures. In fact, we can simply simulate a small data set of dielectric unit cells and use transfer learning to fine tune the simulator. Without a significant change of other parts in the framework, our method will

be capable of designing complex, multifunctional dielectric metasystems.

With the generator and the simulator working on the unit cells of single-layer nanostructures, the optimizer assembles unit cells into multilayers. The unit cells at the same planar position but on different layers can be collectively viewed as a supercell of the metasystem, and the overall performance of the supercell is calculated by the matrixchain multiplication of the wave matrix of each unit cell and the spacers in between. In one iteration, the ES optimizer will optimize one layer of the supercell and keep other layers unaltered. After the selection, reproduction, mutation, and elimination processes of the evolutionary algorithm, the optimizer will select the nanostructure which leads to the least discrepancy between the optical response of the supercell and the predefined objective. In the next iteration, the framework will optimize the next layer of the supercell (from the top layer to the bottom, then back to top). The loop will proceed until satisfactory performance of the supercell is obtained, then the framework will work on designing the supercells at other planar positions. Compared to other optimization methods for multilayer metasurfaces, our ES optimizer needs no sub-objective of every layer but instead optimizes the supercell toward an overall objective, which is more efficient and avoids the null-space problem of the solutions to the sub-objectives. Network architectures and training details of our DL algorithm framework are presented in the Supporting Information.

ASSOCIATED CONTENT

3 Supporting Information

The Supporting Information is available free of charge at https://pubs.acs.org/doi/10.1021/acsnano.0c09424.

Structures and training details of the CPPN-GAN. Structures and training details of the NN simulator. Wave-matrix method for multiple-layer structures. Shape tolerance in experiment. High-resolution structure of the dual-functional Bessel—Airy beam generator. Theoretical model of the all-optical second-order differentiator. High-resolution structure of the all-optical second-order differentiator. Structures of the 256 unique supercells of the space-polarization-wavelength multiplexed hologram. High-resolution output images of the space-polarization-wavelength multiplexed hologram. Discussion on the hologram performance and capacity. Additional examples of the space-polarization-wavelength multiplexed hologram (PDF)

AUTHOR INFORMATION

Corresponding Author

Wenshan Cai — School of Electrical and Computer Engineering, Georgia Institute of Technology, Atlanta, Georgia 30332, United States; School of Materials Science and Engineering, Georgia Institute of Technology, Atlanta, Georgia 30332, United States; orcid.org/0000-0002-6367-3857; Email: wcai@gatech.edu

Authors

Dayu Zhu – School of Electrical and Computer Engineering, Georgia Institute of Technology, Atlanta, Georgia 30332, United States

Zhaocheng Liu — School of Electrical and Computer Engineering, Georgia Institute of Technology, Atlanta, Georgia 30332, United States; orcid.org/0000-0001-6623-9231

Lakshmi Raju – School of Electrical and Computer Engineering, Georgia Institute of Technology, Atlanta, Georgia 30332, United States Andrew S. Kim – School of Electrical and Computer Engineering, Georgia Institute of Technology, Atlanta, Georgia 30332, United States

Complete contact information is available at: https://pubs.acs.org/10.1021/acsnano.0c09424

Notes

The authors declare no competing financial interest.

ACKNOWLEDGMENTS

This work was supported in part by the Office of Naval Research under grant no. N00014-17-1-2555 and by the National Science Foundation under grant no. DMR-2004749. L.R. acknowledges the support of the National Science Foundation Graduate Research Fellowship under grant no. DGE-1650044. A.S.K. acknowledges support from the Department of Defense NDSEG Fellowship Program.

REFERENCES

- (1) Yu, N.; Capasso, F. Flat Optics with Designer Metasurfaces. *Nat. Mater.* **2014**, *13*, 139–150.
- (2) Bomzon, Z. e.; Biener, G.; Kleiner, V.; Hasman, E. Space-Variant Pancharatnam-Berry Phase Optical Elements with Computer-Generated Subwavelength Gratings. *Opt. Lett.* **2002**, *27*, 1141–1143.
- (3) Aieta, F.; Kats, M. A.; Genevet, P.; Capasso, F. Multiwavelength Achromatic Metasurfaces by Dispersive Phase Compensation. *Science* **2015**, 347, 1342–1345.
- (4) Wang, S.; Wu, P. C.; Su, V.-C.; Lai, Y.-C.; Chen, M.-K.; Kuo, H. Y.; Chen, B. H.; Chen, Y. H.; Huang, T.-T.; Wang, J.-H.; et al. A Broadband Achromatic Metalens in the Visible. *Nat. Nanotechnol.* **2018**, *13*, 227–232.
- (5) Jang, M.; Horie, Y.; Shibukawa, A.; Brake, J.; Liu, Y.; Kamali, S. M.; Arbabi, A.; Ruan, H.; Faraon, A.; Yang, C. Wavefront Shaping with Disorder-Engineered Metasurfaces. *Nat. Photonics* **2018**, *12*, 84–90
- (6) Li, L.; Ruan, H.; Liu, C.; Li, Y.; Shuang, Y.; Alù, A.; Qiu, C.-W.; Cui, T. J. Machine-Learning Reprogrammable Metasurface Imager. *Nat. Commun.* **2019**, *10*, 1082.
- (7) Brongersma, M. L.; Shalaev, V. M. The Case for Plasmonics. *Science* **2010**, 328, 440–441.
- (8) Lin, D.; Fan, P.; Hasman, E.; Brongersma, M. L. Dielectric Gradient Metasurface Optical Elements. *Science* **2014**, 345, 298–302.
- (9) Wang, B.; Dong, F.; Li, Q.-T.; Yang, D.; Sun, C.; Chen, J.; Song, Z.; Xu, L.; Chu, W.; Xiao, Y.-F.; et al. Visible-Frequency Dielectric Metasurfaces for Multiwavelength Achromatic and Highly Dispersive Holograms. *Nano Lett.* **2016**, *16*, 5235–5240.
- (10) Wen, D.; Yue, F.; Li, G.; Zheng, G.; Chan, K.; Chen, S.; Chen, M.; Li, K. F.; Wong, P. W. H.; Cheah, K. W.; et al. Helicity Multiplexed Broadband Metasurface Holograms. *Nat. Commun.* **2015**, *6*, 8241.
- (11) Mehmood, M.; Mei, S.; Hussain, S.; Huang, K.; Siew, S.; Zhang, L.; Zhang, T.; Ling, X.; Liu, H.; Teng, J.; et al. Visible-Frequency Metasurface for Structuring and Spatially Multiplexing Optical Vortices. *Adv. Mater.* **2016**, *28*, 2533–2539.
- (12) Raeker, B. O.; Grbic, A. Compound Metaoptics for Amplitude and Phase Control of Wave Fronts. *Phys. Rev. Lett.* **2019**, *122*, 113901.
- (13) Zhou, Y.; Zheng, H.; Kravchenko, I. I.; Valentine, J. Flat Optics for Image Differentiation. *Nat. Photonics* **2020**, *14*, 316–323.
- (14) Camayd-Muñoz, P.; Ballew, C.; Roberts, G.; Faraon, A. Multifunctional Volumetric Meta-Optics for Color and Polarization Image Sensors. *Optica* **2020**, *7*, 280–283.
- (15) LeCun, Y.; Bengio, Y.; Hinton, G. Deep Learning. *Nature* **2015**, 521, 436–444.
- (16) Donahue, J.; Anne Hendricks, L.; Guadarrama, S.; Rohrbach, M.; Venugopalan, S.; Saenko, K.; Darrell, T. Long-Term Recurrent Convolutional Networks for Visual Recognition and Description. Proceedings of the IEEE Conference on Computer Vision and Pattern

- Recognition, Boston, MA, June 7-12, 2015, IEEE: New York, 2015; pp 2625-2634.
- (17) He, K.; Zhang, X.; Ren, S.; Sun, J. Deep Residual Learning for Image Recognition. Proceedings of the *IEEE Conference on Computer Vision and Pattern Recognition*, Las Vegas, NV, June 27–30, 2016; IEEE: New York, 2016; pp 770–778.
- (18) Carleo, G.; Troyer, M. Solving the Quantum Many-Body Problem with Artificial Neural Networks. Science 2017, 355, 602–606.
- (19) Shen, D.; Wu, G.; Suk, H.-I. Deep Learning in Medical Image Analysis. *Annu. Rev. Biomed. Eng.* **2017**, *19*, 221–248.
- (20) Sanchez-Lengeling, B.; Aspuru-Guzik, A. Inverse Molecular Design Using Machine Learning: Generative Models for Matter Engineering. *Science* **2018**, *361*, 360–365.
- (21) Peurifoy, J.; Shen, Y.; Jing, L.; Yang, Y.; Cano-Renteria, F.; DeLacy, B. G.; Joannopoulos, J. D.; Tegmark, M.; Soljačić, M. Nanophotonic Particle Simulation and Inverse Design Using Artificial Neural Networks. *Sci. Adv.* **2018**, *4*, No. eaar4206.
- (22) Malkiel, I.; Mrejen, M.; Nagler, A.; Arieli, U.; Wolf, L.; Suchowski, H. Plasmonic Nanostructure Design and Characterization via Deep Learning. Light: Sci. Appl. 2018, 7, 60.
- (23) Liu, D.; Tan, Y.; Khoram, E.; Yu, Z. Training Deep Neural Networks for the Inverse Design of Nanophotonic Structures. *ACS Photonics* **2018**, *5*, 1365–1369.
- (24) Jiang, J.; Fan, J. A. Global Optimization of Dielectric Metasurfaces Using a Physics-Driven Neural Network. *Nano Lett.* **2019**, *19*, 5366–5372.
- (25) Ma, W.; Cheng, F.; Xu, Y.; Wen, Q.; Liu, Y. Probabilistic Representation and Inverse Design of Metamaterials Based on a Deep Generative Model with Semi-Supervised Learning Strategy. *Adv. Mater.* **2019**, *31*, 1901111.
- (26) Li, Y.; Xu, Y.; Jiang, M.; Li, B.; Han, T.; Chi, C.; Lin, F.; Shen, B.; Zhu, X.; Lai, L.; et al. Self-Learning Perfect Optical Chirality *via* a Deep Neural Network. *Phys. Rev. Lett.* **2019**, 123, 213902.
- (27) Molesky, S.; Lin, Z.; Piggott, A. Y.; Jin, W.; Vucković, J.; Rodriguez, A. W. Inverse Design in Nanophotonics. *Nat. Photonics* **2018**, *12*, 659–670.
- (28) An, S.; Fowler, C.; Zheng, B.; Shalaginov, M. Y.; Tang, H.; Li, H.; Zhou, L.; Ding, J.; Agarwal, A. M.; Rivero-Baleine, C.; et al. A Deep Learning Approach for Objective-Driven All-Dielectric Metasurface Design. ACS Photonics 2019, 6, 3196–3207.
- (29) Liu, Z.; Zhu, D.; Rodrigues, S. P.; Lee, K.-T.; Cai, W. Generative Model for the Inverse Design of Metasurfaces. *Nano Lett.* **2018**, *18*, 6570–6576.
- (30) So, S.; Rho, J. Designing Nanophotonic Structures Using Conditional Deep Convolutional Generative Adversarial Networks. *Nanophotonics* **2019**, *8*, 1255–1261.
- (31) Kiarashinejad, Y.; Abdollahramezani, S.; Adibi, A. Deep Learning Approach Based on Dimensionality Reduction for Designing Electromagnetic Nanostructures. *npj Comput. Mater.* **2020**, *6*, 12.
- (32) Hegde, R. S. Photonics Inverse Design: Pairing Deep Neural Networks with Evolutionary Algorithms. *IEEE J. Sel. Top. Quantum Electron.* **2020**, *26*, 1–8.
- (33) Bayati, E.; Pestourie, R.; Colburn, S.; Lin, Z.; Johnson, S. G.; Majumdar, A. Inverse Designed Metalenses with Extended Depth of Focus. *ACS Photonics* **2020**, *7*, 873–878.
- (34) Goodfellow, I.; Pouget-Abadie, J.; Mirza, M.; Xu, B.; Warde-Farley, D.; Ozair, S.; Courville, A.; Bengio, Y. Generative Adversarial Nets. *Twenty-eighth Conference on Neural Information Processing Systems*, Montreal, Canada, December 8–13, 2014; Neural Information Processing Systems: San Diego, CA, 2014; pp 2672–2680.
- (35) LeCun, Y.; Bottou, L.; Bengio, Y.; Haffner, P. Gradient-Based Learning Applied to Document Recognition. *Proc. IEEE* **1998**, *86*, 2278–2324.
- (36) Liu, Z.; Zhu, D.; Lee, K. T.; Kim, A. S.; Raju, L.; Cai, W. Compounding Meta-Atoms into Metamolecules with Hybrid Artificial Intelligence Techniques. *Adv. Mater.* **2020**, *32*, 1904790.

- (37) Stanley, K. O. Compositional Pattern Producing Networks: A Novel Abstraction of Development. *Genet. Program. Evolvable Mach.* **2007**, *8*, 131–162.
- (38) Silva, A.; Monticone, F.; Castaldi, G.; Galdi, V.; Alù, A.; Engheta, N. Performing Mathematical Operations with Metamaterials. *Science* **2014**, 343, 160–163.
- (39) Zhu, T.; Zhou, Y.; Lou, Y.; Ye, H.; Qiu, M.; Ruan, Z.; Fan, S. Plasmonic Computing of Spatial Differentiation. *Nat. Commun.* **2017**, *8*, 15391.
- (40) Zhou, J.; Qian, H.; Chen, C.-F.; Zhao, J.; Li, G.; Wu, Q.; Luo, H.; Wen, S.; Liu, Z. Optical Edge Detection Based on High-Efficiency Dielectric Metasurface. *Proc. Natl. Acad. Sci. U. S. A.* **2019**, *116*, 11137–11140.
- (41) Feldmann, J.; Youngblood, N.; Wright, C.; Bhaskaran, H.; Pernice, W. All-Optical Spiking Neurosynaptic Networks with Self-Learning Capabilities. *Nature* **2019**, *569*, 208–214.
- (42) Kwon, H.; Sounas, D.; Cordaro, A.; Polman, A.; Alù, A. Nonlocal Metasurfaces for Optical Signal Processing. *Phys. Rev. Lett.* **2018**, *121*, 173004.
- (43) Ni, X.; Kildishev, A. V.; Shalaev, V. M. Metasurface Holograms for Visible Light. *Nat. Commun.* **2013**, *4*, 2807.
- (44) Ozaki, M.; Kato, J.-i.; Kawata, S. Surface-Plasmon Holography with White-Light Illumination. *Science* **2011**, 332, 218–220.
- (45) Huang, L.; Mühlenbernd, H.; Li, X.; Song, X.; Bai, B.; Wang, Y.; Zentgraf, T. Broadband Hybrid Holographic Multiplexing with Geometric Metasurfaces. *Adv. Mater.* **2015**, 27, 6444–6449.
- (46) Li, X.; Chen, L.; Li, Y.; Zhang, X.; Pu, M.; Zhao, Z.; Ma, X.; Wang, Y.; Hong, M.; Luo, X. Multicolor 3D Meta-Holography by Broadband Plasmonic Modulation. *Sci. Adv.* **2016**, *2*, No. e1601102.
- (47) Makey, G.; Yavuz, Ö.; Kesim, D. K.; Turnalı, A.; Elahi, P.; Ilday, S.; Tokel, O.; Ilday, F. Ö. Breaking Crosstalk Limits to Dynamic Holography Using Orthogonality of High-Dimensional Random Vectors. *Nat. Photonics* **2019**, *13*, 251–256.